ANNUAL REPORT, 2007

Project: Elastoplastic dynamics of non-planar faults

PIs: Steven M. Day (San Diego State University) and Benchun Duan (now at Texas A &M University)

1. PROJECT OVERVIEW

Ground motion intensity measures such as peak velocity and response spectral ordinates are bounded above because of physical limits on: (1) fault friction, which limits the density of stored strain energy prior to rupture, and (2) the strength of geological materials, which limits the amplitude of stress wave disturbances excited by rupture and propagated to sites of interest. These strength limits lead to nonlinear deformation off the fault surface, and this deformation can interact strongly with irregularities in fault geometry to modify rupture processes and seismic radiation. We use dynamic rupture simulations to study ground motion extremes in the presence of interactions between complex fault geometry and rupture-induced nonlinear deformation, as a step toward the objective of applying the methodology to site-specific assessment of ground motion extremes for Solitario Canyon fault scenarios at Yucca Mountain.

2. SUMMARY OF 2007 RESULTS

As an initial example of off-fault damage distribution near fault irregularities, and the resulting effects on seismic radiation, we model 2D strike-slip faults with a kink.

Figure 1 gives the fault geometry and stations at which the x-component particle velocities will be shown in a later figure (Figure 4). The 2D right-lateral strike-slip fault has a kink (a change of 10° in the strike) at the coordinate of x = 10000 m and y = 0 m. The rupture starts at x = 7000 m and propagates bilaterally. Six stations are labeled by their azimuth with respect to the fault kink and are on a concentric circle with a distance from the kink of 1 km. The initial stress field is uniform in the entire model with $\sigma_{xx} = \sigma_{yy} =$ 100 MPa and $\sigma_{xy} =$ 45 MPa. Static and dynamic frictional coefficients on the fault are 0.6 and 0.3, respectively. A linear slip-weakening friction law with the critical slip distance of 0.15 m is used and the rupture is artificially initiated within a 660 m long patch within which a fixed rupture speed of 2000 m/s is assigned. Outside of this initiation patch, the rupture propagates spontaneously.

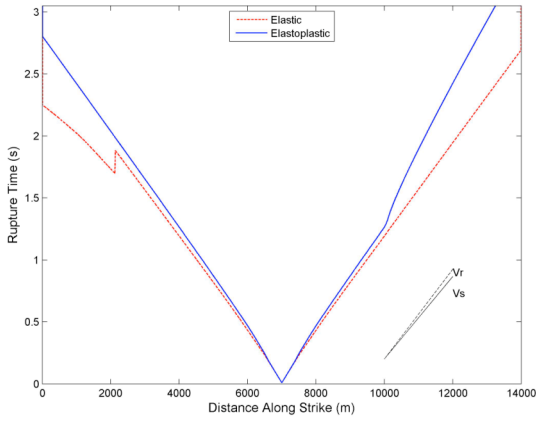

Figure 2. Rupture time on the kinked fault in "elastic" and "elastoplastic" calculations.

Figure 2 shows rupture time in two calculations: off-fault response is purely elastic in one calculation ("elastic") and it is Mohr-Coulomb elastoplastic in the other calculation ("elastoplastic"). In the latter calculation, the

internal coefficient of friction and cohesion are chosen as 0.75 and 0 MPa, respectively. The 10° change in the fault strike does not significantly decelerate the rupture in the elastic calculation, while it slows down the rupture in the elastoplastic calculation. Supershear rupture only occurs to the left of the nucleation point in the elastic calculation.

Figure 2 shows rupture time in two calculations: off-fault response is purely elastic in one calculation ("elastic") and it is Mohr-Coulomb elastoplastic in the other calculation ("elastoplastic"). In the latter calculation, the internal coefficient of friction and cohesion are chosen as 0.75 and 0 MPa, respectively. The 10° change in the fault strike does not significantly decelerate the rupture in the elastic calculation, while it slows down the rupture in the elastoplastic calculation. Supershear rupture only occurs to the left of the nucleation point in the elastic calculation.

Figure 3 shows the distribution of off-fault plastic strain magnitude to the right of rupture initiation in the elastoplastic calculation. Distinct features are associated with the fault kink. The most prominent feature is the long plastic strain band that extends more than 600 m from the fault kink. Plastic strain in this band is significantly larger than that of the surroundings, particularly away from the fault. This localized strain band may represent a spontaneously generated subsidiary fault during the coseismic period, accommodating the change of slip direction at the fault kink. In addition, there are several plastic strain lobes with large plastic strain that may represent extensive cracking near the kink. There is another, shorter plastic strain band to the right of the kink, which is subparallel to the above long band and may represent another, shorter subsidiary fault. We have shown (Duan and Day, 2007) that the kink-induced plastic strain distribution shown in Figure 3, although highly localized into bands, is practically grid-independent (although this is not the case with the shear banding that sometimes develops spontaneously, far from discrete geometrical features, e.g., Duan and Day, 2006, Templeton and Rice, 2007).

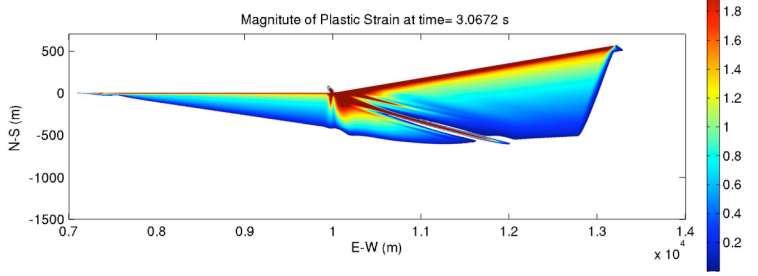

Figure 3. The distribution of off-fault plastic strain magnitude in the elastoplastic calculation of the kinked fault. Distinct features are associated with the fault kink.

Figure 4 shows the x-component of particle velocity at the six stations shown in Figure 1. These stations are 1 km away from the fault kink and are labeled by their azimuth with respect to the kink. To better understand the kink radiation, we also perform calculations on a planar fault that is along y = 0 m, without the change in the fault strike. Departures of particle velocities from the planar fault result are primarily due to the kink radiation. One important feature evident at Stations S, SW, and NW is that the localized plastic yielding near the kink significantly reduces high frequencies of the kink radiation. If off-fault response is purely elastic, a velocity step (which controls the high frequency asymptote of the seismic radiation from the kink) is predicted theoretically (Adda-Bedia and Madariaga, 2007) for antiplane rupture, and can be observed at

these three stations (solid red curves) for our elastic in-plane simulations (at approximately 1.5 s). The abruptness of the steps in the elastic case is limited only by the grid resolution (element size was 5 m in the above calculations). Off-fault plastic yielding smoothes the velocity step, introducing a longer rise time and reducing high-frequency radiation. The reduction is significant above several Hertz. However, the above feature is not obvious at the stations N, NE, and SE. Furthermore, off-fault plastic yielding appears to make particle velocity at stations NE and SE more complex. We are continuing to analyze these simulations to better understand the azimuthal variations in the kink radiation in the presence of off-fault plastic yielding.

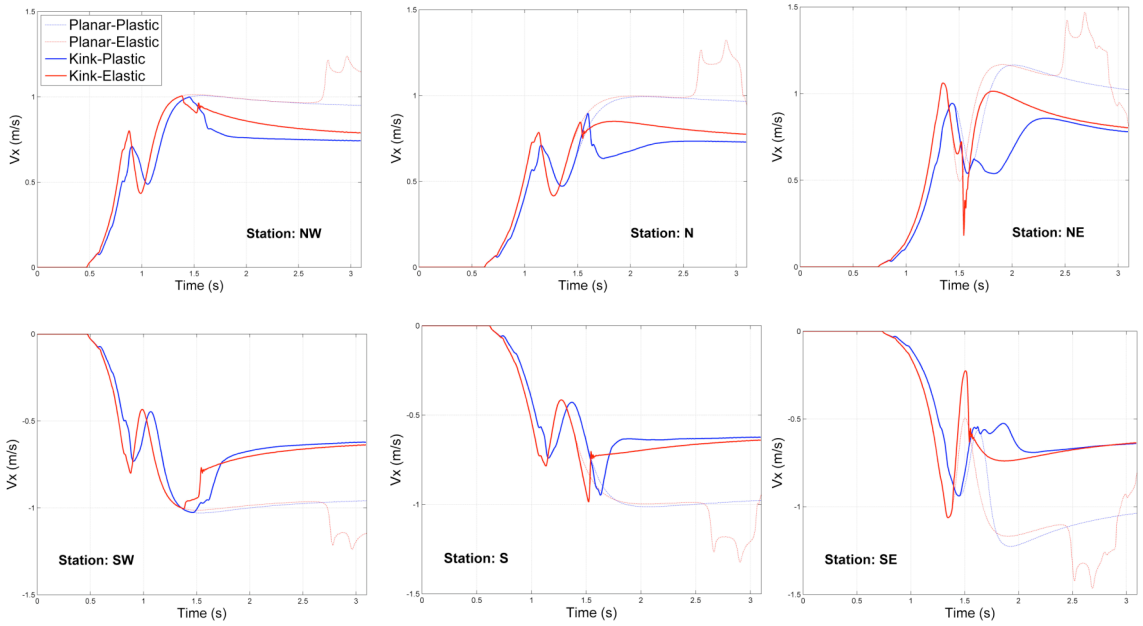

Figure 4. X-component of particle velocity at six stations shown in Figure 1. Elastic (red curves) and Elastoplastic (blue curves) calculations are performed on the kinked fault (heavy solid curves) of Figure 1 and a planar fault (light dash-dot curves) that is along y = 0 m without change in strike. Departures from planar fault curves are due to kink radiations.

3. REFERENCES

Adda-Bedia, M and R. Madariaga (2007), Seismic radiation from a kink on an antiplane fault, *Bull. Seismol. Soc. Am.*, in press.

Duan, B., and S. M. Day (2006). Elastoplastic dynamic analysis of strike-slip faults with bends using finite element method, AGU 2006 Annual Meeting, San Francisco, CA, December 11-15, 2006.

Duan, B., and S. M. Day (2007). Modeling the reduction of high-frequency seismic radiation due to plastic strain localization at fault kinks, SCEC 2007 Annual Meeting, Palm Springs, CA, September 8-12, 2007.

Templeton, E. L. and J. R. Rice (2007), Localization of deformation in elastic-plastic analysis of dynamic shear rupture, *2007 SCEC Annual Meeting*, Palm Springs, California.